This article has been accepted for publication in a future issue of this journal, but has not been fully edited. Content may change prior to final publication. Citation information: DOI 10.1109/LSP.2016.2606760, IEEE Signal Processing Letters

SAR Image Segmentation with Rényi's Entropy

Ricardo H. Nobre[a], Francisco A. A. Rodrigues[a], Regis C. P. Marques[b], Juvêncio S. Nobre[c], Jeová F. S. R. Neto[a], Fátima N. S. Medeiros[a].

***Abstract*—SAR image segmentation is an important task in image processing. However, classic segmentation techniques are inadequate due to the presence of speckle noise. In this paper, we present a methodology for SAR image segmentation that uses the matrix of Rényi's entropy. This matrix arises from SAR data that follows the G_A^0 model and here it is an input to segmentation methods. For performance evaluation of the proposed methodology, we employ the Error of Segmentation, the Cross-Region Fitting index, the Dice measure, as well as the rates of false positives and negatives. Tests have been performed on synthetic and real SAR images and the matrix of entropy has improved the results, regardless of the increase of the number of looks. The Otsu's method of global thresholding produced good segmentation results when applied to this matrix.**

***Index Terms*—SAR image, segmentation, Rényi's entropy, G_A^0 distribution.**

I. Introduction

SYNTHETIC Aperture Radar (SAR) has been used for many years in activities related to global earth monitoring. There are many advantages of using SAR systems when compared to standard optical ones, since they operate independently of the weather and of the presence of sunlight conditions [1]–[4]. However, due to the coherent illumination of these systems, SAR images suffer strong contamination by speckle noise [5]–[7]. In fact, this interference significantly degrades the quality of SAR images, which leads to difficulty in image processing tasks [3], [8], [9].

Statistical approaches are generally required to deal with the speckle noise. Thus, the choice of an appropriate probability distribution to model SAR data plays an important role in image segmentation. The Gamma, Weibull and *K* distributions are widely used in the literature for SAR data modeling [10]. However, none of these has the flexibility to model adequately homogeneous, heterogeneous and extremely heterogeneous regions based on SAR image amplitudes as the G_A^0 distribution [10]–[12].

Aiming at improving and generating higher accurate segmentation results, several approaches have been developed for SAR images such as binary partition trees (BPT) [13], mean-shift (MS) algorithm [14], clustering based methods [15]–[17], to name but a few examples. Recently, the roughness information of SAR image arose as an important attribute to drive image segmentation [15], [18]. Rodrigues *et al.* [18] introduced the roughness map (M_α) of the data model, estimated by the method of log-cumulants (MoLC), as input to segmentation methods based on thresholding and level set methods. Although the data model is also specified by the scale parameter, Rodrigues *et al.* employed only the roughness. A shortcoming of this approach is that the segmentation performance substantially decays with the increase in the number of looks. It is noteworthy that, as the number of looks increases, the speckle noise reduces as well as the roughness [18]. Moreover, this approach tends to mis-segment regions with the same α and different γ as only one region. Therefore, these limitations denote that both parameters are essential for SAR image processing and target characterization [11], [19]. An interesting segmentation algorithm should consider all the parameters of the distribution used as the data model. In particular, the concept of Rényi's entropy is an alternative tool for SAR image segmentation [20] and optical image processing [21] to overcome the aforementioned limitations.

In this paper, we introduce the matrix of Rényi's entropy ($MoRE$), for data modeled by the G_A^0 distribution, to drive SAR image segmentation. In order to validate the use of $MoRE$, we carried out experiments with the Otsu's method [22] and *K*-means clustering algorithm [23] and two other methods based on level sets [24], [25].

II. The G_A^0 Distribution for Speckled Data

The amplitude return (Z) of the speckled data is modeled by the G_A^0 distribution [11]:

$$f_{G_A^0}(z,\alpha,\gamma,L) = \frac{2L^L\Gamma(L-\alpha)}{\gamma^\alpha\Gamma(-\alpha)\Gamma(L)}\frac{z^{2L-1}}{(\gamma+Lz^2)^{L-\alpha}}, \quad (1)$$

where $-\alpha$, $\gamma, z > 0$, $L \geq 1$ and the rth order non-central moment is given by

$$E_{G_A^0}[Z^r] = \left(\frac{\gamma}{L}\right)^{\frac{r}{2}}\frac{\Gamma(-\alpha-\frac{r}{2})\Gamma(L+\frac{r}{2})}{\Gamma(-\alpha)\Gamma(L)}, \quad \alpha < -\frac{r}{2}. \quad (2)$$

The parameters α, γ and L correspond to the roughness, scale and number of looks, respectively. In this paper, L is assumed known and constant for all pixels of the image.

A. Parameter Estimation of the G_A^0 Model

To estimate the parameters of the G_A^0 distribution, we can use the method of moments (MoM) [11], [26] and the modified method of moments [27], maximum likelihood (ML) [28], robust estimators [29], and the more recent log-cumulants

This research was supported by CNPq and CAPES under grant numbers 401442/2014-4 and 444784/2014-4 to which the authors are thankful.

[a] Corresponding author: UFC - Teleinformatics Engineering Department - 60455-760, Fortaleza,CE - Brazil. E-mail: rhnobre@gmail.com, alixandreavila@gmail.com, jeovafarias@gmail.com, fsombra@ufc.br

[b] IFCE - Telematic Department - Fortaleza,CE - Brazil. E-mail: regismarques@ifce.edu.br

[c] UFC - Department of Statistics and Applied Mathematics - 60455-760, Fortaleza,CE - Brazil. E-mail: juvencio@ufc.br

This article has been accepted for publication in a future issue of this journal, but has not been fully edited. Content may change prior to final publication. Citation information: DOI 10.1109/LSP.2016.2606760, IEEE Signal Processing Letters

(MoLC) [12], [18], [30]. These techniques have specific limitations [30], mainly related to their analytical solutions and numerical problems [25].

In this paper, we apply MoM for parameter estimation of G_A^0 because it provides consistent estimates [25], [31] and it is computationally fast [18]. To avoid strong data blurring [28], we use small windows to estimate the parameters. The parameter estimation through MoM was achieved by solving the relation between the sample moments ($\widehat{m}_r$) and the theoretical ($E_{G_A^0}[Z^r]$) of order r, where $r \in \{1/2, 1\}$ [25]:

$$\frac{\Gamma^2(-\widehat{\alpha}-1/4)}{\Gamma(-\widehat{\alpha})\Gamma(-\widehat{\alpha}-1/2)} - \frac{\widehat{m}_{1/2}^2}{\widehat{m}_1}\frac{\Gamma(L)\Gamma(L+1/2)}{\Gamma^2(L+1/4)} = 0. \quad (3)$$

The scale parameter $\widehat{\gamma}$ is obtained by replacing α in Eq. (2) by $\widehat{\alpha}$, putting $r = 1$ and $E_{G_A^0}[Z] = \widehat{m}_1$.

III. The Rényi's Entropy of the G_A^0 Model

The differential Rényi's entropy of a distribution P with probability density function f is given by [32], [33]

$$H_q(P) = \frac{1}{1-q}\ln\int f^q(w)\,\mathrm{d}w, \quad (4)$$

where $q \in \mathbb{R}^+ - \{1\}$. If $q \to 1$, the Rényi's entropy tends to the Shannon's entropy [34]. The parameter q is essential to adjust the sensitivity of the entropy to the shape of the probability density function [35]. Furthermore, it enables the Rényi's entropy to obtain several measurements of similarity within the same family of distributions [36].

For the G_A^0 distribution, the differential Rényi's entropy is given by

$$H_q(G_A^0) = \frac{1}{1-q}\ln\int_0^\infty \left[\frac{2L^L\Gamma(L-\alpha)}{\gamma^\alpha\Gamma(L)\Gamma(-\alpha)} z^{(2L-1)} \left(\gamma + Lz^2\right)^{\alpha-L}\right]^q \mathrm{d}z. \quad (5)$$

Since there is not closed form for Eq. (5), its solution requires numerical integration methods. In this paper, $MoRE$ is obtained via Eq. (5) for each image pixel. An important aspect of $MoRE$, based on G_A^0 distribution, is that its histogram indicates the number of image regions regardless of an increase in the number of looks. Since $MoRE$ is suitable for discriminating regions, it can also be used to guide segmentation methods.

Figs. 1 (a), (b), (c) and (d) illustrate synthetic SAR images, simulated by G_A^0, with different number of regions, and with the parameter setting $\alpha \in \{-1.5; -4; -8; -12\}$, $\gamma \in \{0.005; 0.2; 2; 20\}$ and $L \in \{1; 8\}$. Figs. 1 (e), (f), (g) and (h) depict the well defined modes in the histograms which are appropriate inputs for SAR image segmentation based on thresholding methods.

IV. The Proposed Methodology

The flowchart of the proposed methodology for SAR image segmentation based on $MoRE$ is illustrated in Fig. 2. We can see in Fig. 2 that the image histogram is unsuitable to determine the number of regions that compose the input image. The parameter estimation is performed pixel by pixel through the MoM in a 5x5 window. In fact, large windows are inadequate to estimate the parameters in heterogeneous areas [28]. The matrices of estimated parameters $(\widehat{\alpha}, \widehat{\gamma})$ are then used to compute the Rényi's entropy, according to Eq. (5) and the $MoRE$. Finally, the $MoRE$ and its histogram (e.g., thresholds) are inputs to the segmentation methods. Here, we determine the threshold value, T_{RE}, by applying the Otsu's method [22] to $MoRE$.

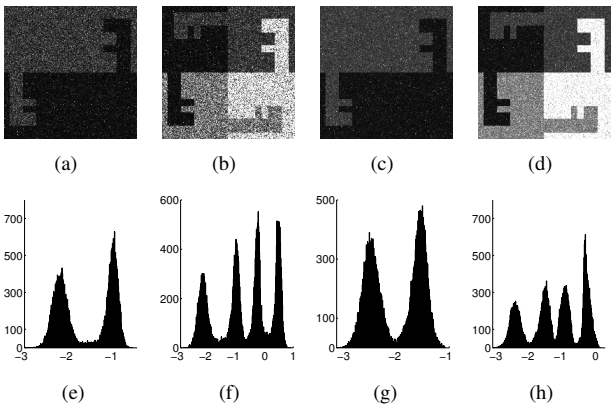

Fig. 1. SAR images in amplitude with different number of regions: (a) and (b) 2 and 4 regions (1 look), respectively; (c) and (d) 2 and 4 regions (8 looks), respectively; and (e)-(h) the corresponding $MoRE$ histograms.

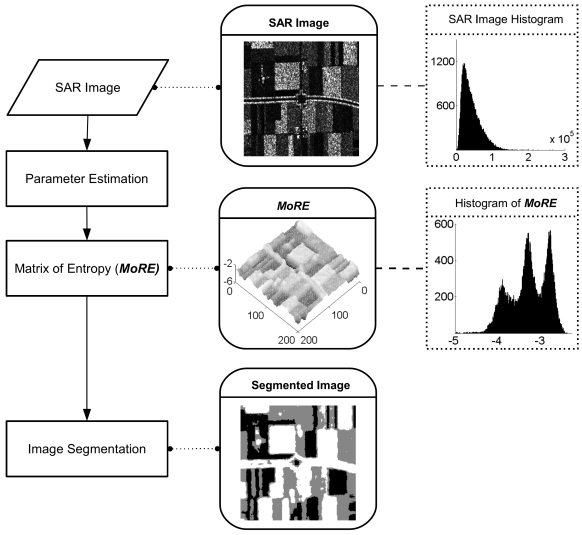

Fig. 2. Flowchart of the proposed methodology.

A. Level Set Related Methods

We performed tests with the Otsu and *K*-means algorithms for image segmentation and clustering, respectively and we assessed two other segmentation methods based on level sets.

1) The Modified Huang et al. Method: Huang *et al.* [24] have proposed a level set energy function F based on the intensity level of the pixel $I(l, c)$, where l and c stand for the line and column, respectively. Here, we modify this method by replacing $I(l, c)$ by $MoRE(l, c)$, and the thresholds $I_{average}$, I_{lower} and I_{higt} by T_{RE}.

This article has been accepted for publication in a future issue of this journal, but has not been fully edited. Content may change prior to final publication. Citation information: DOI 10.1109/LSP.2016.2606760, IEEE Signal Processing Letters

2) The Modified Marques et al. Method: Marques *et al.* [25] have designed a level set approach for SAR image segmentation based on the statistical properties of image regions that are modeled by a G_A^0 distribution. The modified version consists in replacing the energy function in [25] by $MoRE$.

V. Results and Discussion

A. Measures for Image Segmentation Evaluation

Here, we apply the Error of Segmentation (EoS) index to evaluate the performance of the proposed methodology on synthetic images. This index is defined by

$$EoS = \frac{\#(E)}{\#(Image)}, \tag{6}$$

where $\#(E)$ is the number of mis-segmented pixels and $\#(Image)$ is the total number of image pixels. We also used the false positive rate (FPR), false negative rate (FNR), and $Dice$ [37], [38].

For real SAR images, for which the ground truths are unknown, we aply two measures to quantify the quality and difficulty of the segmentation. The Cross-Region Fitting (CRF), which lies within the interval [0, 1], quantifies the segmentation accuracy. Here, $CRF = 1$ indicates the best segmentation. DoS measures the difficulty of segmentation based on the contrast between a region foreground and background. When the region contrast is low, the value of DoS is high [25].

B. Simulated SAR Data

A Monte Carlo experiment was conducted for synthetic SAR data following a G_A^0 distribution, varying the number of looks $\{L \in \mathbb{Z}^+ : 1 \leq L \leq 8\}$. We used 45 binary images of different sizes and shapes, where the foreground (f) and background (b) regions follow the $G_A^0(\alpha_f, \gamma_f, L)$ and $G_A^0(\alpha_b, \gamma_b, L)$ distributions, respectively. In this context, the following scenarios were evaluated: (a) $\alpha_f = \alpha_b$ and $\gamma_f \neq \gamma_b$; (b) $\alpha_f \neq \alpha_b$ and $\gamma_f = \gamma_b$ and (c) $\alpha_f \neq \alpha_b$ and $\gamma_f \neq \gamma_b$. The scenarios use the following parameters: $\alpha \in \{-1.5, -4, -8\}$, $\gamma \in \{1, 20, 40\}$ and $L \in \{1, 2, \cdots, 8\}$ which yield 576 different combinations with 25920 different tests. To improve the robustness, we submitted the same image 1000 times for each test.

Inspired by [25], we simulated synthetic amplitude SAR images by using:

$$Z = \sqrt{-\frac{\gamma}{\alpha}\Upsilon^{-1}_{2L,-2\alpha}(U)}, \tag{7}$$

where $\Upsilon^{-1}_{2L,-2\alpha}$ is the inverse cumulative distribution function of Snedecor's F law with $2L$ and -2α degrees of freedom, and U is a uniformly distributed random variable in $(0, 1)$.

After estimating the G_A^0 parameters, we assessed q and EoS, simultaneously. Although there are special cases where $q \in \{0^+, 1^+, 2\}$, there is not an exact rule to setting q. Thus, we empirically set $q = 4$, since it achieved the lowest value of EoS for the critical case where the speckle is stronger, i.e. L=1, as Fig. 3 shows.

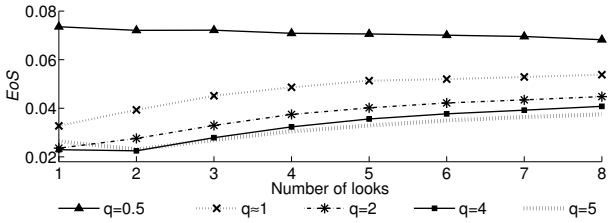

Fig. 3. EoS measure for different values of q.

The relation between EoS and L, in Fig. 4, for synthetic images demonstrates the segmentation accuracy by using the Rényi's entropy of the G_A^0 distribution, although L has increased.

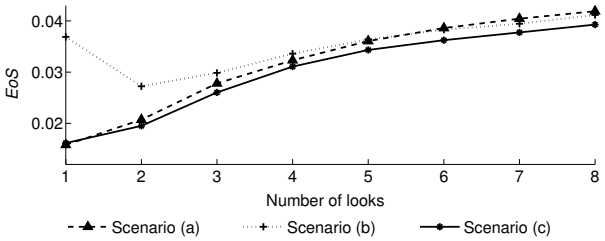

Fig. 4. EoS measure for the three scenarios.

Fig. 5 exhibits the edge maps of segmentation results from a Monte Carlo experiment by applying the Otsu's method to the $MoRE$ of synthetic images.

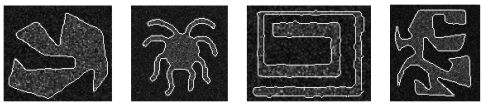

Fig. 5. Segmentation results of the Monte Carlo experiment.

Fig. 6 shows the empirical cumulative distribution function (ecdf) of the evaluation measures by applying a Monte Carlo experiment to synthetic images. The plots show that the slope of the ecdf curve is proportional to the segmentation accuracy. The Otsu's method achieved high probability of EoS, FPR and $FNR < 0.1$ and low probability of the $Dice$ index < 0.85. Thus, the results demonstrated the ability of the method to segment speckled images driven by $MoRE$.

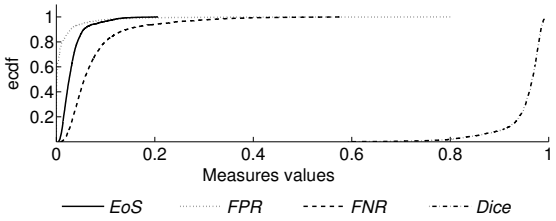

Fig. 6. The ecdf curves of the evaluation measures.

The low values of FPR and FNR indicate that the methods accomplished high values of true positive rate (sensitivity) and true negative rate (specificity). The results demonstrated

This article has been accepted for publication in a future issue of this journal, but has not been fully edited. Content may change prior to final publication. Citation information: DOI 10.1109/LSP.2016.2606760, IEEE Signal Processing Letters

that our methodology incorporated significant information into the segmentation process and hence it reduced the occurrence of false positives and false negatives. The low value of EoS and the high similarity $Dice$ index confirm these results. Table I strengthens the results shown in Fig. 6.

TABLE I
MEAN ± STANDARD DEVIATION FOR THE OTSU'S METHOD.

EoS ↓	***FPR*** ↓	***FNR*** ↓	***Dice*** ↑
0.032 ± 0.025	0.012 ± 0.040	0.077 ± 0.069	0.953 ± 0.046

The synthetic data analysis supports that our methodology based on $MoRE$ is feasible for SAR image segmentation and furthermore to drive methods based on level sets.

C. Real SAR Data

We have applied the proposed method to real SAR images. Fig. 7(a) shows part of Vancouver, Canada (400x400 pixels, 1 look, HH by the RADARSAT-2), while Fig. 7(c) displays a region in Sanchagang, China (512x512 pixels, 3 looks, HH by the TerraSAR-X).

(a) (b) (c) (d)

Fig. 7. (a) and (c) refer to real SAR images in amplitude and (b) and (d) correspond to the best segmentation result employing $MoRE$.

Table II displays the comparative results by using the CRF measure for the segmentation methods. The CRF index shows the proposed methodology presented the least segmentation error. These results also indicate that the proposed methodology significantly improved SAR image segmentation when compared to the methods in [22], [23] and [24] applied to SAR data. We also compared our methodology to the algorithms introduced in [18] and [25] which perform over the the roughness parameter map and the SAR image energy map, respectively. Thus, the performance evaluation demonstrated the suitability and efficacy of $MoRE$ for SAR image segmentation, although there is an increase in the number of looks. Actually, the histogram of $MoRE$ favored the performance of the Otsu and the *K*-means methods. We performed the experiments on a 3.1 GHz CPU with 8 GB RAM using MatLab. Table III presents the computational time for the segmentation process.

TABLE II
DOS AND CROSS-REGION FITTING FOR REAL IMAGES.

Images	***DoS***	**Applied to**	**Methods**			
			[22]	[23]	[24]	[25]
Vancouver (1 look)	0.543	SAR Data	0.444	0.435	0.552	0.619[a]
		M_α [18]	0.741	0.737	0.668	0.684
		$MoRE$	**0.805**	**0.791**	**0.702**	**0.690**
China (3 looks)	0.387	SAR Data	0.798	0.793	0.801	0.827[a]
		M_α [18]	0.885	0.885	0.882	0.881
		$MoRE$	**0.899**	**0.896**	**0.891**	**0.890**

[a]Segmentation processed over the SAR image energy map proposed in [25].

TABLE III
COMPUTATIONAL TIME FOR REAL IMAGES IN SECONDS.

Images	**Applied to**	**Methods**			
		[22]	[23]	[24]	[25]
Vancouver (1 look)	SAR Data	0.242	1.444	42.659	40.145
	M_α [18]	>3000	>3000	>3000	>3000
	$MoRE$	**105.993**	**106.728**	**130.200**	**126.270**
China (3 looks)	SAR Data	0.310	0.670	26.337	0.253
	M_α [18]	>6000	>6000	>6000	>6000
	$MoRE$	**118.583**	**118.994**	**134.281**	**137.040**

For real SAR images, Table II and Table III show that the proposed methodology improved the segmentation results without substantially overloading the processing time.

Fig. 8 exemplifies that $MoRE$ is also suitable to perform multiple region segmentation of SAR image.

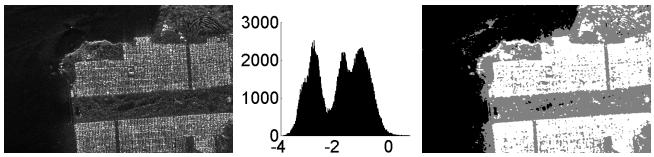

(a) (b) (c)

Fig. 8. (a) San Francisco image (600x450 pixels, 4 looks, HH by AIRSAR); (b) the $MoRE$ histogram and (c) segmentation result with Otsu over $MoRE$.

VI. CONCLUSIONS

In this paper, we introduced a segmentation methodology based on the Rényi's entropy of SAR data modeled by the G_A^0 distribution. The Monte Carlo experiments with synthetic images showed satisfactory results which demonstrated that the proposed methodology incorporated meaningful information into the segmentation process. The performance evaluation of the real SAR image results also confirmed the advantage of using the Rényi's entropy based approach. Among the advantages of the our methodology we can list: the ability of $MoRE$ to identify different image regions since it encompasses the parameters (α,γ) of the data model (G_A^0); the increase in the number of looks slightly affects the segmentation performance; the methodology presented promising results and it improved the performance of both methods based on level sets. Moreover, $MoRE$ may also drive other SAR image processing techniques, such as filtering and classification. A disadvantage of this methodology is that there is not a closed form for the Rényi's entropy of G_A^0, and hence it requires the use of numerical integration methods.

Further work will investigate the application of our methodology to SAR data modeled by other distributions.

REFERENCES

[1] K. Tomiyasu, "Tutorial review of synthetic-aperture radar (SAR) with applications to imaging of the ocean surface," *Proc. IEEE*, vol. 66, no. 5, pp. 563–583, May 1978.

[2] E. S. Kasischke, J. M. Melack, and M. C. Dobson, "The use of imaging radars for ecological applications - A review," *Remote Sens. of Environment*, vol. 59, no. 2, pp. 141–156, Feb. 1997.

[3] M. Silva, F. Cribari-Neto, and A. C. Frery, "Improved likelihood inference for the roughness parameter of the GA0 distribution," *Environmetrics*, vol. 19, no. 4, pp. 347–368, Aug. 2008.

[4] G. Dong, N. Wang, and G. Kuang, "Sparse representation of monogenic signal: With application to target recognition in SAR images," *IEEE Signal Process. Lett.*, vol. 21, no. 8, pp. 952–956, Aug. 2014.

[5] J.-S. Lee, "Speckle analysis and smoothing of synthetic aperture radar images," *Comput. Graph. and Image Process.*, vol. 17, no. 1, pp. 24–32, Sep. 1981.

[6] ——, "Speckle suppression and analysis for synthetic aperture radar images," *Optical Engineering*, vol. 25, no. 5, pp. 636–643, May 1986. [Online]. Available: http://dx.doi.org/10.1117/12.7973877

[7] C. Lopez-Martinez and X. Fabregas, "Polarimetric SAR speckle noise model," *IEEE Trans. Geosci. Remote Sens.*, vol. 41, no. 10, pp. 2232–2242, Oct. 2003.

[8] F. Galland, J. M. Nicolas, H. Sportouche, M. Roche, F. Tupin, and P. Refregier, "Unsupervised synthetic aperture radar image segmentation using Fisher distributions," *IEEE Trans. Geosci. Remote Sens.*, vol. 47, no. 8, pp. 2966–2972, Aug. 2009.

[9] R. C. P. Marques, F. N. S. Medeiros, and D. Ushizima, "Target detection in SAR images based on a level set approach," *IEEE Trans. Syst., Man, Cybern., Syst.*, vol. 39, no. 2, pp. 214–222, Mar. 2009.

[10] G. Gao, "Statistical modeling of SAR images: A survey," *Sensors*, vol. 10, no. 1, pp. 775–795, 2010.

[11] A. C. Frery, H. J. Müller, C. C. Freitas, and S. J. S. Sant'Anna, "A model for extremely heterogeneous clutter," *IEEE Trans. Geosci. Remote Sens.*, vol. 35, no. 3, pp. 648–659, May 1997.

[12] J. Feng, Z. Cao, and Y. Pi, "Multiphase SAR image segmentation with G^0 statistical-model-based active contours," *IEEE Trans. Geosci. Remote Sens.*, vol. 51, no. 7, pp. 4190–4199, Jul. 2013.

[13] A. Alonso-Gonzalez, C. Lopez-Martinez, and P. Salembier, "Filtering and segmentation of polarimetric SAR data based on binary partition trees," *IEEE Trans. Geosci. Remote Sens.*, vol. 50, no. 2, pp. 593–605, Feb. 2012.

[14] P. Jarabo-Amores, M. Rosa-Zurera, D. de la Mata-Moya, R. Vicen-Bueno, and S. Maldonado-Bascon, "Spatial-range mean-shift filtering and segmentation applied to SAR images," *IEEE Trans. Instrum. Meas.*, vol. 60, no. 2, pp. 584–597, Feb. 2011.

[15] X. Tian, L. Jiao, L. Yi, K. Guo, and X. Zhang, "The image segmentation based on optimized spatial feature of superpixel," *J. Vis. Commun. Image R.*, vol. 26, pp. 146–160, Jan. 2015.

[16] R. Shang, P. Tian, L. Jiao, R. Stolkin, J. Feng, B. Hou, and X. Zhang, "A spatial fuzzy clustering algorithm with kernel metric based on immune clone for SAR image segmentation," *IEEE J. Sel. Topics Appl. Earth Observ. in Remote Sens.*, vol. 9, no. 4, pp. 1640–1652, Apr. 2016.

[17] F. Liu, Y. Duan, L. Li, L. Jiao, J. Wu, S. Yang, X. Zhang, and J. Yuan, "SAR image segmentation based on hierarchical visual semantic and adaptive neighborhood multinomial latent model," *IEEE Trans. Geosci. Remote Sens.*, vol. 54, no. 7, pp. 4287–4301, Jul. 2016.

[18] F. A. A. Rodrigues, J. F. S. R. Neto, R. C. P. Marques, F. N. Medeiros, and J. S. Nobre, "SAR image segmentation using the roughness information," *IEEE Geosci. Remote Sens. Lett.*, vol. 13, no. 2, pp. 146–160, Feb. 2016.

[19] O. H. Bustos, M. M. Lucini, and A. C. Frery, "M-Estimators of roughness and scale for G^0_A-modelled SAR imagery," *EURASIP J. Adv. Sig. Pr.*, vol. 2002, no. 1, pp. 1–10, 2002.

[20] A. C. Frery, R. J. Cintra, and A. D. C. Nascimento, "Entropy-based statistical analysis of PolSAR data," *IEEE Trans. Geosci. Remote Sens.*, vol. 51, no. 6, pp. 3733–3743, Jun. 2013.

[21] P. K. Sahoo and G. Arora, "A thresholding method based on two-dimensional Rényi's entropy," *Pattern Recognition*, vol. 37, no. 6, pp. 1149 – 1161, Jun. 2004. [Online]. Available: http://www.sciencedirect.com/science/article/pii/S0031320303004023

[22] N. Otsu, "A threshold selection method from gray-level histograms," *IEEE Trans. Syst. Cybern.*, vol. 9, no. 1, pp. 62–66, Jan. 1979.

[23] J. MacQueen, "Some methods for classification and analysis of multivariate observations," in *Proc. of the Fifth Berkeley Symp. on Math. Statist. and Probability*, 1967, pp. 281–297.

[24] B. Huang, H. Li, and X. Huang, "A level set method for oil slick segmentation is SAR images," *Int. J. Remote Sens.*, vol. 26, no. 6, pp. 1145–1156, Mar. 2005.

[25] R. C. P. Marques, F. N. Medeiros, and J. S. Nobre, "SAR image segmentation based on level set approach and G^0_A model," *IEEE Trans. Pattern Anal. Mach. Intell.*, vol. 34, no. 10, pp. 2046–2057, Oct. 2012.

[26] J. Gambini, M. E. Mejail, J. Jacobo, and A. Frery, "Accuracy of edge detection methods with local information in speckled imagery," *Stat. Comput.*, vol. 18, no. 1, pp. 15–26, Mar. 2008.

[27] H. Cui, T. Liu, Y. Jiang, and J. Gao, "Parameter estimation for polarimetric synthetic aperture radar imagery based on the $z^r \log z$ moments," *J. of Appl. Remote Sens.*, vol. 9, no. 1, May 2015.

[28] A. C. Frery, F. Cribari-Neto, and M. O. de Souza, "Analysis of minute features in speckled imagery with maximum likelihood estimation," *EURASIP J. Adv. Sig. Pr.*, vol. 2004, no. 16, pp. 2476–2491, Jun. 2004.

[29] H. Allende, A. C. Frery, J. Galbiati, and L. Pizarro, "M-estimators with asymmetric influence functions: The G^0_A distribution case," *J. Stat. Comput. Sim.*, vol. 76, no. 11, pp. 941–956, 2006.

[30] Z. W. Zhu, J. J. Zhou, and Y. Y. Guo, "A MoLC+MoM-based G^0 distribution parameter estimation method with application to synthetic aperture radar target detection," *J. of Central South Univ.*, vol. 22, no. 6, pp. 2207–2217, Jun. 2015. [Online]. Available: http://dx.doi.org/10.1007/s11771-015-2745-x

[31] P. K. Sen, J. M. Singer, and A. C. P. de Lima, *From Finite Sample to Asymptotic Methods in Statistics*, ser. Cambridge Series in Statistical and Probabilistic Math. Cambridge Univ. Press, 2010.

[32] B. Chen, P. Zhu, and J. C. Principe, "Survival information potential: A new criterion for adaptive system training," *IEEE Trans. on Signal Process.*, vol. 60, no. 3, pp. 1184–1194, Mar. 2012.

[33] T. V. Erven and P. Harremoës, "Rényi divergence and Kullback-Leibler divergence," *IEEE Trans. Inf. Theory*, vol. 60, no. 7, pp. 3797–3820, Jul. 2014.

[34] A. Rényi, "On measures of entropy and information," *Proc. of the Fourth Berkeley Symp. on Math. Statist. and Probability*, vol. 1, pp. 547–561, 1961.

[35] T. Maszczyk and W. Duch, *Comparison of Shannon, Rényi and Tsallis Entropy Used in Decision Trees*. Springer Berlin Heidelberg, 2008, pp. 643–651.

[36] J. Kapur, *Measures of Information and Their Applications*. New Delhi, India: John Wiley & Sons, 1994.

[37] L. R. Dice, "Measures of the amount of ecologic association between species," *Ecology*, vol. 26, no. 3, pp. 297–302, 1945.

[38] M. Yadollahi, A. Procházka, M. Kašparová, O. Vyšata, and V. Mařík, "Separation of overlapping dental arch objects using digital records of illuminated plaster casts," *BioMedical Engineering OnLine*, vol. 14, no. 1, pp. 1–15, Jul. 2015. [Online]. Available: http://dx.doi.org/10.1186/s12938-015-0066-9